The transcriptional regulator CCCTC-binding factor limits oxidative stress in endothelial cells

Received for publication, August 28, 2017, and in revised form, March 28, 2018 Published, Papers in Press, April 2, 2018, DOI 10.1074/jbc.M117.814699

Anna R. Roy[‡§], Abdalla Ahmed[‡§], Peter V. DiStefano[¶], Lijun Chi[‡], Nadiya Khyzha[¶], Niels Galjart[‖], Michael D. Wilson[§], Jason E. Fish[¶‡‡§§1], and Paul Delgado-Olguín[‡§ §§2]**

*From the [‡]Translational Medicine Research Program, The Hospital for Sick Children, Toronto, Ontario M5G 0A4, Canada, [§]Department of Molecular Genetics, University of Toronto, Toronto, Ontario M5S 1A8, Canada, [¶]Toronto General Hospital Research Institute, University Health Network, Toronto, Ontario M5G 2C4, Canada, [‖]Department of Cell Biology and Genetics, Erasmus Medical Center, Rotterdam 3015 CN, The Netherlands, **Genetics and Genome Biology Research Program, The Hospital for Sick Children, Toronto, Ontario M5G 0A4, Canada, [‡‡]Department of Laboratory Medicine and Pathobiology, University of Toronto, Toronto, Ontario M5S 1A8, Canada, and [§§]Heart and Stroke Richard Lewar Centre of Excellence in Cardiovascular Research, Toronto, Ontario M5S 3H2, Canada*

Edited by Velia M. Fowler

The CCCTC-binding factor (CTCF) is a versatile transcriptional regulator required for embryogenesis, but its function in vascular development or in diseases with a vascular component is poorly understood. Here, we found that endothelial Ctcf is essential for mouse vascular development and limits accumulation of reactive oxygen species (ROS). Conditional knockout of *Ctcf* in endothelial progenitors and their descendants affected embryonic growth, and caused lethality at embryonic day 10.5 because of defective yolk sac and placental vascular development. Analysis of global gene expression revealed *Frataxin* (*Fxn*), the gene mutated in Friedreich's ataxia (FRDA), as the most strongly down-regulated gene in Ctcf-deficient placental endothelial cells. Moreover, *in vitro* reporter assays showed that Ctcf activates the *Fxn* promoter in endothelial cells. ROS are known to accumulate in the endothelium of FRDA patients. Importantly, Ctcf deficiency induced ROS-mediated DNA damage in endothelial cells *in vitro*, and in placental endothelium *in vivo*. Taken together, our findings indicate that Ctcf promotes vascular development and limits oxidative stress in endothelial cells. These results reveal a function for Ctcf in vascular development, and suggest a potential mechanism for endothelial dysfunction in FRDA.

The CCCTC-binding factor (CTCF)[3] is a highly conserved versatile transcriptional regulator that interacts with DNA and multiple protein partners (1–3). CTCF is mainly known for its function as a genomic insulator, and as a mediator of long-range genomic interactions (1, 4–7); however, it can also promote gene expression as a member of transcriptional activation complexes (1, 3). Constitutive Ctcf depletion in mice results in death during early embryogenesis (8). We are only beginning to understand how Ctcf controls specific mammalian development processes (7, 9–14). For instance, Ctcf interacts with myogenic master regulators to control myogenic cell differentiation and muscle development (2, 3). In addition, Ctcf acts as a mediator of long-range genomic interactions to control limb and heart development (6, 9, 14). Overexpression experiments revealed that CTCF limits retinal angiogenesis by preventing enhancer-mediated activation of the gene encoding vascular endothelial growth factor (*VEGF*) (15). Whether CTCF controls development of the vascular system has not been investigated.

Development of the mouse vasculature begins during gastrulation at embryonic day (E) 6.5 with migration of a subpopulation of mesodermal precursors from the primitive streak toward the embryo proper and extraembryonic tissues, *i.e.* the yolk sac and placenta (16–19). Development of the vascular network begins with formation of new vessels by vasculogenesis, followed by branching of preexisting vessels by angiogenesis in the yolk sac (16). Blood starts circulating after formation of the primitive vascular plexus in the yolk sac and the embryo proper at E8.25, promoting vascular plexus remodeling into a complex network (16). Vasculogenesis after chorioallantoic fusion at E8.0 initiates placental vascular development, and branching angiogenesis forms a complex placental vascular network known as the labyrinth, which mediates nutrient and gas exchange between the mother and the developing embryo (16, 17). Endothelial transcriptional programs coordinate vascular development (18–21). Transcriptional misregulation in endothelial cells in embryonic and extra embryonic vascula-

This work was funded by the Natural Sciences and Engineering Research Council of Canada (NSERC) Grant 500865 (to P. D. O). This work was also supported by the Heart and Stroke Foundation of Canada Grant G-17–0018613, the Canadian Institutes of Health Research (CIHR) Grant PJT-149046, and Operational Funds from the Hospital for Sick Children (to P. D. O.) and from the Canadian Institutes of Health Research (CIHR) Grant MOP-119506 (to J. E. F).The authors declare that they have no conflicts of interest with the contents of this article.

This article contains Figs. S1–S7 and Table S1.

[1] Holder of a Canada Research Chair from Canadian Institutes of Health Research.

[2] To whom correspondence should be addressed: 686 Bay St., Toronto, Ontario M5G 0A4, Canada. Tel.: 416-813-5080; Fax: 416-813-7480; E-mail: paul.delgadoolguin@sickkids.ca.

[3] The abbreviations used are: CTCF, CCCTC-binding factor; E, embryonic day; FRDA, Friedreich's ataxia; ROS, reactive oxygen species; eNOS, endothelial nitric-oxide synthase; BAEC, bovine aortic endothelial cell; HUVEC, human umbilical vein endothelial cells; 8-OHG, 8-hydroxyguanosine; 4HNA, 4-hydroxynonenal; PFA, paraformaldehyde; qPCR, quantitative PCR.

ture can cause cardiac and vascular defects leading to disease (22, 23).

Friedreich's ataxia (FRDA) is the most common hereditary neurodegenerative disease (24). Vascular defects and endothelial dysfunction may contribute to FRDA. Impaired vascularization might contribute to muscle fatigability (25). In addition, cardiomyopathy in FRDA is associated with microvascular disease (26). Furthermore, FRDA patients exhibit decreased flow-mediated dilation in the brachial artery, suggesting that endothelial dysfunction may contribute to FRDA (27). FRDA is caused by abnormal expansion of GAA trinucleotide repeats at intron 1 of the *Frataxin* (*FXN*) gene that results in decreased protein levels (28), and increased levels of reactive oxygen species (ROS) and oxidative stress (29, 30). FXN is a mitochondrial protein involved in the assembly of iron and sulfur clusters (31) expressed mainly in tissues with high metabolic rates, such as the heart and brown fat (32). GAA trinucleotide repeat expansion triggers silencing of *FXN* gene expression via epigenetic mechanisms (33). For instance, in FRDA patients' cells and mouse models, histones located near the expanded GAA repeats are occupied with the repressive mark histone H3 lysine 9 trimethylation (H3K9me3), and have reduced levels of acetylated core histones, which mark transcriptionally active genes (34–36). These modifications might interfere with the activity of transcriptional regulators controlling *FXN* expression. Studies on fibroblasts and cerebellum from FRDA patients showed that CTCF binding is required to maintain transcriptionally active chromatin, as its depletion from the 5′ untranslated region (5′-UTR) of *FXN* results in heterochromatin formation. Whether CTCF controls *FXN* gene expression in endothelial cells, and regulates vascular development is unknown.

Results

Ctcf is expressed in developing and adult mouse vascular endothelium

Ctcf is broadly expressed (3). However, its expression in embryonic or adult vascular endothelial cells has not been investigated. To visualize Ctcf protein in developing vascular endothelium, we performed immunofluorescence for Ctcf and platelet endothelial cell adhesion molecule 1 (Pecam-1), an endothelial marker, on sagittal sections of mice at E9.5, E11.5, postnatal day 2, and 6-week-old adults. Ctcf was detected in nuclei ubiquitously, and was present in vascular endothelial cell nuclei in the third branchial arch, outflow tract, aorta, and pulmonary artery (Fig. 1*A*). Thus, Ctcf is expressed in vascular endothelial cells throughout embryogenesis and in adulthood.

Ctcf in endothelial progenitors and their derivatives is essential for embryogenesis

Ctcf controls important developmental processes (7, 9–13), but its function in vascular development is unknown. To uncover the function of *Ctcf* in vascular development, we conditionally inactivated *Ctcf* in mouse endothelial progenitors and their derivatives by cre-mediated homologous recombination of a floxed allele. Exons 3 to 12 of *Ctcf* are flanked by *LoxP* sites in the *Ctcf* floxed allele (37), which was crossed with *Tie2-cre* transgenics (38). Efficiency of *Ctcf* depletion in endothelial cells was evaluated by immunofluorescence for Ctcf and

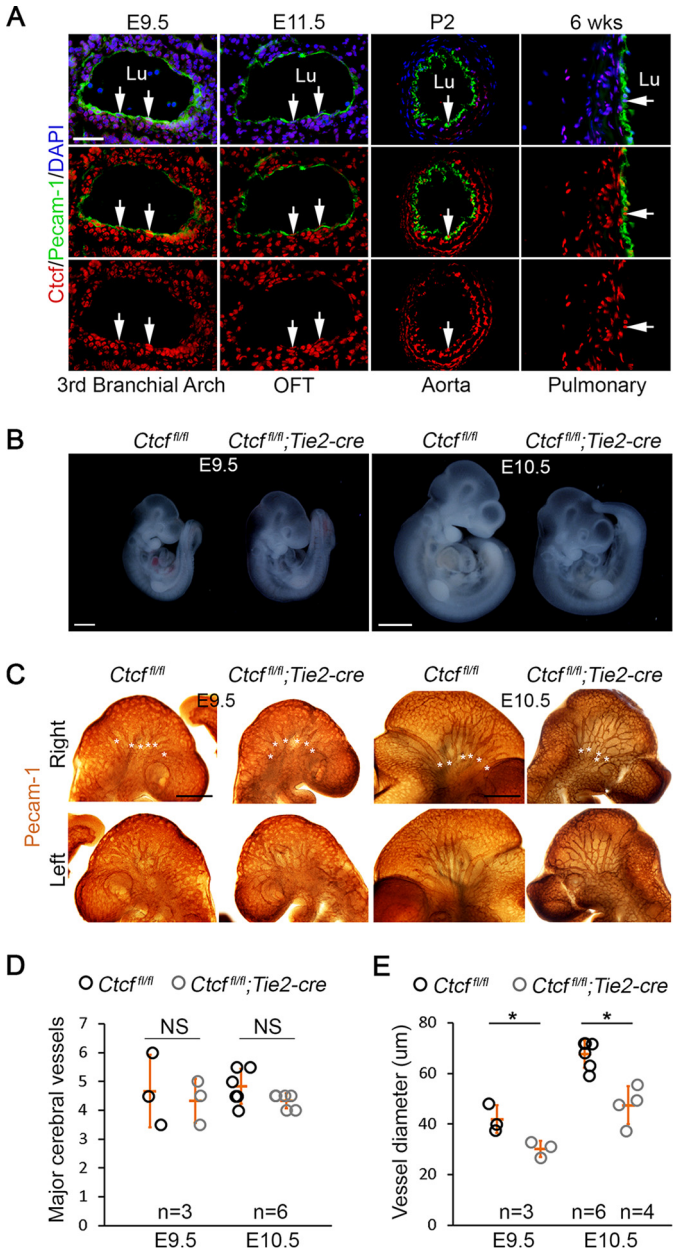

Figure 1. Ctcf in endothelial cells is essential for embryogenesis. *A*, immunostaining of Ctcf (*red*), and Pecam-1 (*green*) on sagittal sections on the third branchial arch, outflow tract (*OFT*), aorta, and pulmonary artery from E9.5, E11.5, postnatal day 2 (*P2*), and 6-week-old adult mice. *Arrows* point to examples of endothelial cells expressing Ctcf. *Lu*, blood vessel lumen. *Scale bar* = 50 μm. *B*, whole control (*Ctcf*$^{fl/fl}$) and *Ctcf* mutant (*Ctcf*$^{fl/fl}$;*Tie2-cre*) embryos at E9.5 and E10.5. *C*, head of control and *Ctcf* mutant embryos at E9.5 and E10.5 stained for Pecam-1 by immunohistochemistry. *White asterisks* indicate major brain vessels. *Scale bars* = 1 mm. *D*, number of major brain vessels in control and *Ctcf* mutant embryos at E9.5 and E10.5. *NS*, nonsignificant. *E*, diameter of brain vessels in control and *Ctcf* mutant embryos at E9.5 and E10.5. *Error bars* represent the mean ± S.D. *, $p < 0.05$.

Pecam-1. *Ctcf* mutants had over 90% fewer cell nuclei that were double positive for Pecam-1 and Ctcf compared with controls (Fig. S1, *A* and *B*).

Embryos with *Ctcf*-deficient endothelial progenitors and derivatives died by E11.5 (Fig. S1*C*). *Ctcf* mutant embryos at E9.5 had no gross morphological defects. E10.5 embryos were smaller (Fig. 1*B*), suggesting deficient growth. Mutants developed an overall normal heart, with normal ventricular wall

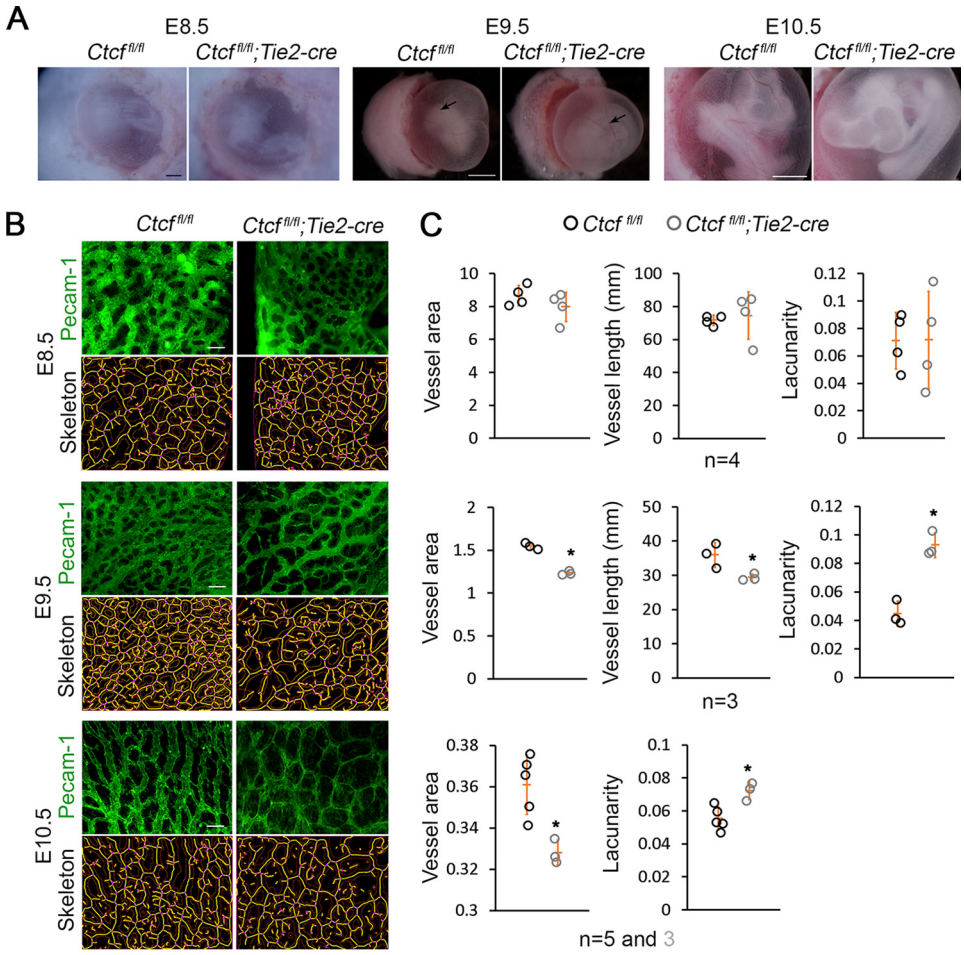

Figure 2. Vascular remodeling defects in yolk sac of Ctcf mutants. *A*, whole mount images of control (*Ctcf*$^{fl/fl}$) and *Ctcf* mutant (*Ctcf*$^{fl/fl}$*;Tie2-cre*) yolk sacs attached to placentae and embryos at E8.5, E9.5, and 10.5. *Scale bar* = 1 mm. *B*, immunofluorescence for Pecam-1 (*green*) on yolk sacs. *Lower panels* are skeletons generated with AngioTool from fluorescent micrographs. *Scale bar* = 100 μm. *C*, quantification of vessel area, total vessel length, and lacunarity from skeletons using AngioTool. *Error bars* represent the mean ± S.D. *, $p < 0.05$.

thickness, but appeared to have reduced trabeculae at E10.5 (Fig. S1, *D* and *E*). To determine whether deficiency of Ctcf affects embryonic vasculature patterning we stained Pecam-1 in whole control and *Ctcf* mutant embryos. *Ctcf* mutants had an overall normal vasculature pattern (Fig. S1*F*). Accordingly, the number of major branches of the cerebral vasculature was comparable between control and mutant embryos at E9.5 and E10.5 (Fig. 1, *C* and *D*). In contrast, quantification of cerebral vessel diameter revealed narrower vessels in *Ctcf* mutants than controls at E9.5 and E10.5 (Fig. 1*E*). Thus, endothelial *Ctcf* is required for embryogenesis and might regulate vascular development.

Ctcf is required for yolk sac vascular remodeling

The developing vascular network extends into the yolk sac and placenta (16). Defects in the yolk sac vasculature can compromise embryonic development (20, 39, 40). Defective yolk sac vasculature might affect embryogenesis in *Ctcf* mutants. To test this possibility, we analyzed the vascular network in the yolk sac of *Ctcf* mutant and control embryos at E8.5, E9.5, and E10.5. *Ctcf* mutant yolk sacs at E8.5 and E9.5 appeared to be properly irrigated, however, E10.5 embryos had a pale yolk sac (Fig. 2*A*), suggesting vascular defects. Immunofluorescence of Pecam-1 in whole yolk sacs revealed the vascular network. We analyzed the yolk sac vascular network in control and *Ctcf* mutants using AngioTool (41). Control and *Ctcf* mutant yolk sacs at E8.5 had comparable vessel area, vessel length and lacunarity, a measure of the average gap between blood vessels and reflective of vessel disorganization (41) (Fig. 2, *B* and *C*). In contrast, E9.5 mutant yolk sacs had a decreased vessel area and vessel length, and increased lacunarity. Similarly, E10.5 *Ctcf* mutant yolk sacs had decreased vessel area and increased lacunarity (Fig. 2, *B* and *C*). These changes were not because of deficient endothelial cell proliferation or increased apoptosis. The number of cells double positive for Pecam-1 and phosphorylated histone H3, were comparable between yolk sacs of control and *Ctcf* mutant embryos at E9.5. Cells double positive for Pecam-1 and activated caspase 3 were absent in control and mutant yolk sacs (Fig. S2).

Blood circulation causes shear stress and induces pressure on blood vessels, stimulating yolk sac vascular remodeling from E8.5 to E9.5 (16, 42). Lack of circulating blood in cultured embryos blocks remodeling of the yolk sac vasculature and causes a dramatic down-regulation of the mechanosensor, endothelial nitric-oxide synthase (eNOS) (encoded by *Nos3*) (16, 42). Deficient yolk sac vascular remodeling in *Ctcf* mutants

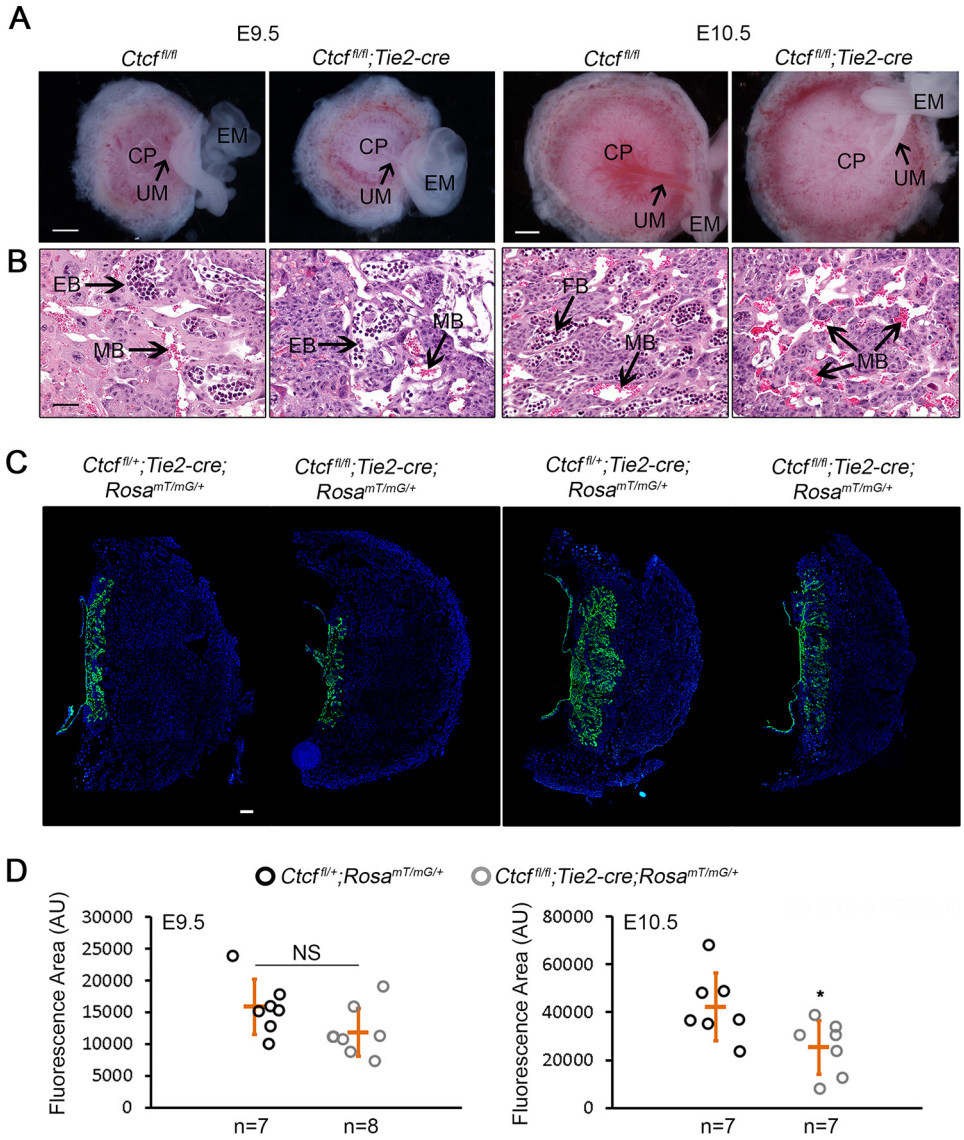

Figure 3. Decreased labyrinth expansion in Ctcf mutants. *A*, whole control (*Ctcf*$^{fl/fl}$) and *Ctcf* mutant (*Ctcf*$^{fl/fl}$*;Tie2-cre*) placentae attached to E9.5 and E10.5 embryos. *Scale bar* = 100 μm. *CP*, chorionic plate; *UM*, umbilical cord; *EM*, embryo. *B*, histological sections of labyrinth. *EB*, embryonic blood; *MB*, maternal blood. *Scale bar* = 50 μm. *C*, GFP (*green*) immunostaining on sections of placentae at E9.5 and E10.5 in control (*Ctcf*$^{fl/+}$*;Tie2-cre;Rosa*$^{mT/mG/+}$) and mutant (*Ctcf*$^{fl/fl}$*;Tie2-cre;Rosa*$^{mT/mG/+}$) embryos. *Scale bar* = 200 μm. *D*, quantification of GFP fluorescence area in E9.5 and E10.5 placentae. *Error bars* represent the mean ± S.D. *NS*, nonsignificant; *AU*, absorbance unit. *, $p < 0.05$.

might be caused by decreased blood flow; therefore, we analyzed the expression of *Nos3* by quantitative PCR (qPCR) and eNOS protein abundance by Western blotting. *Nos3* mRNA, and eNOS protein levels were comparable between control and *Ctcf* mutant yolk sacs at E9.5 (Fig. S3), which agrees with a normally irrigated yolk sac at this stage (Fig. 2*A*). This suggests that vascular remodeling defects in yolk sac up to E9.5 in *Ctcf* mutants are not secondary to decreased blood flow because of heart defects or reduced circulating blood.

Ctcf is required for placental vascular development

Defective labyrinth development can affect embryonic growth (17, 43). Whole placentae still attached to *Ctcf* mutant embryos through the umbilical cord appeared normal at E9.5. However, the placentae and umbilical cords in *Ctcf* mutants appeared improperly irrigated at E10.5 (Fig. 3*A*), suggesting defects in the labyrinth. Accordingly, E9.5 *Ctcf* mutant placentae had both embryonic and maternal blood vessels. In contrast, only maternal blood vessels were observed in histological sections of E10.5 *Ctcf* mutant placentae (Fig. 3*B*). To visualize the labyrinth, we incorporated the cre-dependent GFP reporter *Rosa*$^{mT/mG}$ (44) into *Ctcf* floxed mice carrying the *Tie2-cre* transgene (38), resulting in GFP-labeled endothelial cells. Quantification on placenta sections stained for GFP revealed a comparable labyrinth area in *Ctcf* mutants at E9.5, and a significant decrease at E10.5 (Fig. 3, *C* and *D*). Decreased labyrinth expansion was not caused by decreased endothelial cell proliferation or increased cell death, as the numbers of endothelial cells positive for phosphorylated histone H3, or activated caspase 3, were comparable between control and *Ctcf* mutant placentae at E9.5 and E10.5. Caspase 3–positive cells were absent in E10.5 placentae (Fig. S4). *Nos3* mRNA and eNOS

protein levels were also comparable between control and *Ctcf* mutant placentae at E10.5 (Fig. S3), suggesting that defective labyrinth expansion is not secondary to heart defects or decreased blood flow. Thus, endothelial Ctcf is required for extraembryonic vascular development.

Genome-wide expression profile of E9.5 endothelial cells from WT and Ctcf mutant placentae

To uncover genes and pathways regulating vascular development downstream of Ctcf we performed high-throughput RNA-Seq on endothelial cells sorted from placentae of control (*Ctcf*$^{fl/+}$;*Tie2-cre*;*Rosa*$^{mT/mG/+}$) and *Ctcf* mutant (*Ctcf*$^{fl/fl}$;*Tie2-cre*;*Rosa*$^{mT/mG/+}$) embryos at E9.5. Sorted GFP-positive cells expressed significantly higher levels of *GFP* and the endothelial markers kinase insert domain receptor (*Kdr*), and TEK receptor tyrosine kinase (*Tek*, also known as *Tie2*), than GFP-negative cells (Fig. S5), indicating that the sorted cell population is enriched for endothelial cells. Consistent with loss of Ctcf protein (Fig. S1, *A* and *B*), *Ctcf* mRNA was drastically reduced in endothelial cells sorted from mutant embryos, as shown by qPCR (Fig. S5*B*). RNA-Seq analysis revealed 232 genes that were up-regulated, and 155 genes that were down-regulated over 1.5-fold in *Ctcf* mutant endothelial cells (Fig. 4*A*). Analysis of misregulated genes using DAVID revealed that up-regulated genes are enriched for processes important for vascular development including focal adhesion, extracellular matrix–receptor interaction, and adherens and tight junction. Down-regulated genes are enriched for processes related to cell cycle and genomic stability, and GSH metabolism (Fig. 4*B*). To validate the RNA-Seq results, we performed qPCR on selected genes that were highly misregulated in *Ctcf* mutants, including genes with known functions in vascular development. qPCR was performed on endothelial cells sorted from placentae and yolk sacs from control and *Ctcf* mutant embryos. This analysis confirmed down-regulation of frataxin (*Fxn*), *Gstz1*, *C3ar1*, *E2f2*, *E2f8*, and *Flt4*, and up-regulation of several developmental regulators including *Msx1*, *Tcf7*, *Celsr1*, *Ralgds*, *Pitx1*, *Tead1*, and *Notch1* (Fig. 4, *C* and *D* and Fig. S6). Changes in gene expression levels in placenta, but not yolk sac, were largely consistent with the RNA-Seq (Fig. 4*C*), suggesting that placenta and yolk sac endothelial cells have unique gene expression programs, or that Ctcf controls specific transcriptional pathways in endothelial cells in different organs. RNA-Seq revealed that Frataxin (*Fxn*) was the most down-regulated gene in *Ctcf* mutant placental endothelial cells. Western blotting revealed a slight but statistically significant decrease in Fxn protein in *Ctcf* mutant placentae (Fig. 4, *E* and *F*). This analysis was carried out on labyrinth tissue; therefore, it likely underestimates protein decrease in endothelial cells. qPCR showed dramatic *Fxn* down-regulation consistently in both placental and yolk sac endothelial cells (Fig. 4, *C* and *D*), suggesting that *Fxn* might be a Ctcf target important for vascular endothelial cell development.

CTCF activates the FXN gene promoter

It has been proposed that CTCF activates *FXN* expression by maintaining an open chromatin configuration (33, 45–47). Others and we have shown that Ctcf regulates developmental processes by activating gene expression as a transcription factor (1, 3). To determine whether CTCF activates *FXN* expression as a transcription factor we assessed the capacity of CTCF to activate the *FXN* promoter in an episomal luciferase reporter. Comparison of the 5′ region immediately upstream the mouse *Fxn* gene against a database of validated CTCF-binding sites (48, 49) identified a motif spanning nucleotides −4 to −23 relative to the transcription start site (46). This binding site is conserved in the human *FXN* promoter and has high identity with other previously validated CTCF-binding sites (Fig. 5, *A* and *B*). We cloned a 386-bp DNA fragment corresponding to the 5′ regulatory region of the human *FXN* gene that includes the identified CTCF-binding motif. CTCF significantly activated the *FXN* promoter in transient cotransfections in bovine aortic endothelial cells (BAECs) (Fig. 5*C*). Thus, Ctcf is a transcriptional activator of *FXN* in endothelial cells.

Ctcf prevents oxidative stress in endothelial cells

Frataxin deficiency in yeast (50) and in cells from patients with FRDA causes increased oxidative stress (29, 30), and enhanced oxidative stress is known to negatively affect vascular development (51). Our RNA-Seq analysis revealed that genes down-regulated in *Ctcf* mutant endothelial cells participate in GSH metabolism, including *Fxn* and GSH S-transferase zeta 1 (*Gstz1*) (Fig. 4, *B* and *D*), which modulate ROS generation (52, 53). This suggests a potential function of Ctcf as an oxidative stress regulator. To determine whether Ctcf deficiency causes oxidative stress in endothelium we analyzed ROS-mediated DNA damage in human umbilical vein endothelial cells (HUVECs) with reduced CTCF levels. CTCF was efficiently knocked down in HUVECs using two nonoverlapping siRNAs (Fig. 5, *D* and *E*). CTCF depletion led to decreased levels of *FXN* mRNA (Fig. 5*F*). CTCF-depleted cells were stained using an antibody against 8-hydroxyguanosine (8-OHG), a modified base that occurs in DNA as a result of oxidative stress (54). As positive controls, HUVECs with decreased levels of FXN or treated with H_2O_2 had increased levels of 8-OHG. More CTCF-depleted HUVECs had nuclei that were positive for 8-OHG compared with cells transfected with a control siRNA (Fig. 5, *G* and *H* and Fig. S7). Importantly, enhanced oxidative stress was associated with defects in angiogenesis, as *CTCF* or *FXN* knockdown (Fig. 5*F*) cells had decreased tube length in a Matrigel tube formation assay (Fig. 5, *I* and *J*).

We assessed whether enhanced oxidative stress was also present in *Ctcf* mutant embryos. In sections of placentae at E10.5, significantly more 8-OHG foci were found in endothelial cell nuclei in *Ctcf* mutant embryos, than in controls (Fig. 6, *A* and *B*). Increased ROS promotes lipid peroxidation in a humanized mouse model of FRDA (55). Western blotting revealed increased levels of 4-hydroxynonenal (4HNA), a common byproduct of lipid peroxidation (56), in labyrinth tissue from *Ctcf* mutants compared with controls (Fig. 6, *C* and *D*). Furthermore, endothelial cells in *Ctcf* mutant placentae had higher levels of 4HNA than controls (Fig. 6, *E* and *F*). Thus, Ctcf protects endothelial cells from oxidative stress.

Mitochondrial dysfunction leads to ROS accumulation and lipid peroxidation in a humanized mouse model of FRDA (55). Cytochrome *c*, an essential component of the mitochondrial electron transport chain indispensable for energy production

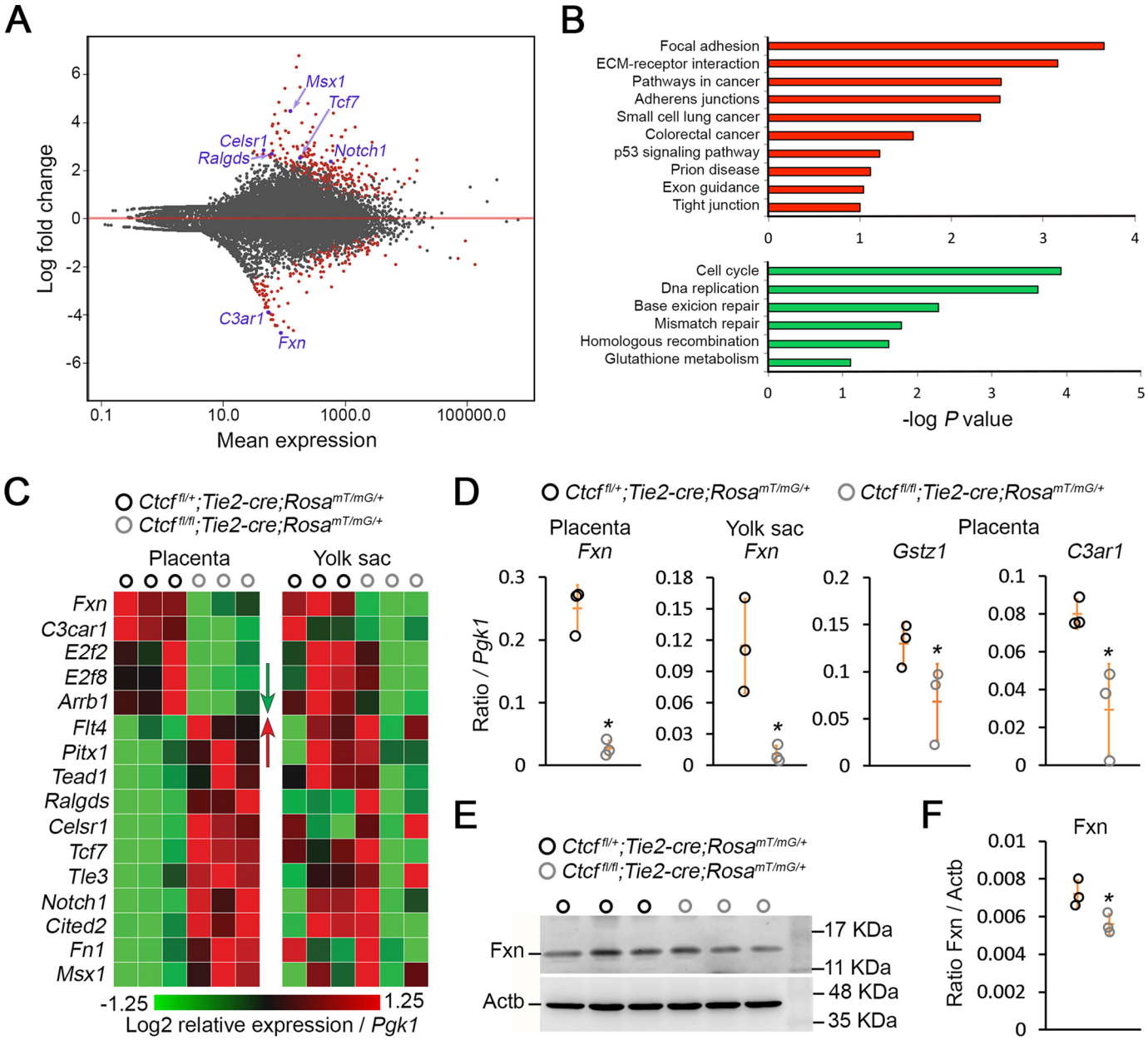

Figure 4. Gene expression profile in Ctcf mutant placental endothelial cells. *A*, MA plot for differential expression in isolated placental labyrinth endothelial cells of control (*Ctcf*$^{fl/+}$;*Tie2-cre*;*Rosa*$^{mT/mG/+}$) and *Ctcf* mutant (*Ctcf*$^{fl/fl}$;*Tie2-cre*;*Rosa*$^{mT/mG/+}$) embryos at E9.5. *Black dots* represent genes with no significant change in expression. *Red dots* represent genes that underwent significant ($p < 0.05$) change in expression. *Blue dots* indicate some of the genes whose misregulation was confirmed by qPCR. *X* axis indicates the normalized mean expression level across all samples, and the *y* axis indicates the log 2-fold change. *B*, gene ontology categories enriched in genes up-regulated (*red*) and down-regulated (*green*) in endothelial cells sorted from control and *Ctcf* mutant placentae at E9.5. *C*, heat map of log 2 expression relative to *Pgk1*, as determined by qPCR on endothelial cells sorted from control and *Ctcf* mutant placentae and yolk sacs, of genes found by RNA-Seq to be misregulated in *Ctcf* mutant placental endothelial cells. *D*, qPCR on endothelial cells sorted from control and *Ctcf* mutant placentae (*Fxn*, *Gstz*, *C3ar1*) and yolk sacs (*Fxn*). Expression levels are relative to *Pgk1*. *E*, Western blotting of Fxn on labyrinths from control and *Ctcf* mutant placentae. Beta actin (*Actb*) was used as loading control. *F*, quantification of band intensities relative to Actb. *Error bars* represent the mean ± S.D. of three biological replicates. *, $p < 0.05$.

(57), is decreased in *FXN* knockdown and mutant cells (58, 59). Accordingly, Western blot analysis showed that cytochrome *c* is decreased in labyrinth tissue from *Ctcf* mutant placentae (Fig. 6, *G* and *H*). The iron-sulfur cluster assembly enzyme (IscU), which regulates mitochondrial iron homeostasis (60), is also decreased in *Fxn* mutant mouse tissues (61). Immunofluorescence on sections of labyrinth from control embryos revealed cytoplasmic and nuclear staining for IscU1 and 2 (IscU1/2) (Fig. 6*I*). This is consistent with cytoplasmic and nuclear localization of IscU1 in mammalian cells; however, the function of iron-sulfur cluster assembly in nucleus is not clear (62). Immunofluorescence revealed decreased levels of IscU1/2 in endothelial nuclei in placentae of *Ctcf* mutant embryos (Fig. 6, *I* and *J*). Thus, similar to FXN-deficient cells, Ctcf deficiency leads to a decrease in cytochrome *c* and IscU proteins.

Discussion

The contribution of Ctcf to vascular growth during development and postnatally remains poorly understood. Previously, it was shown that Ctcf can bind the promoter of *Vegf* to prevent

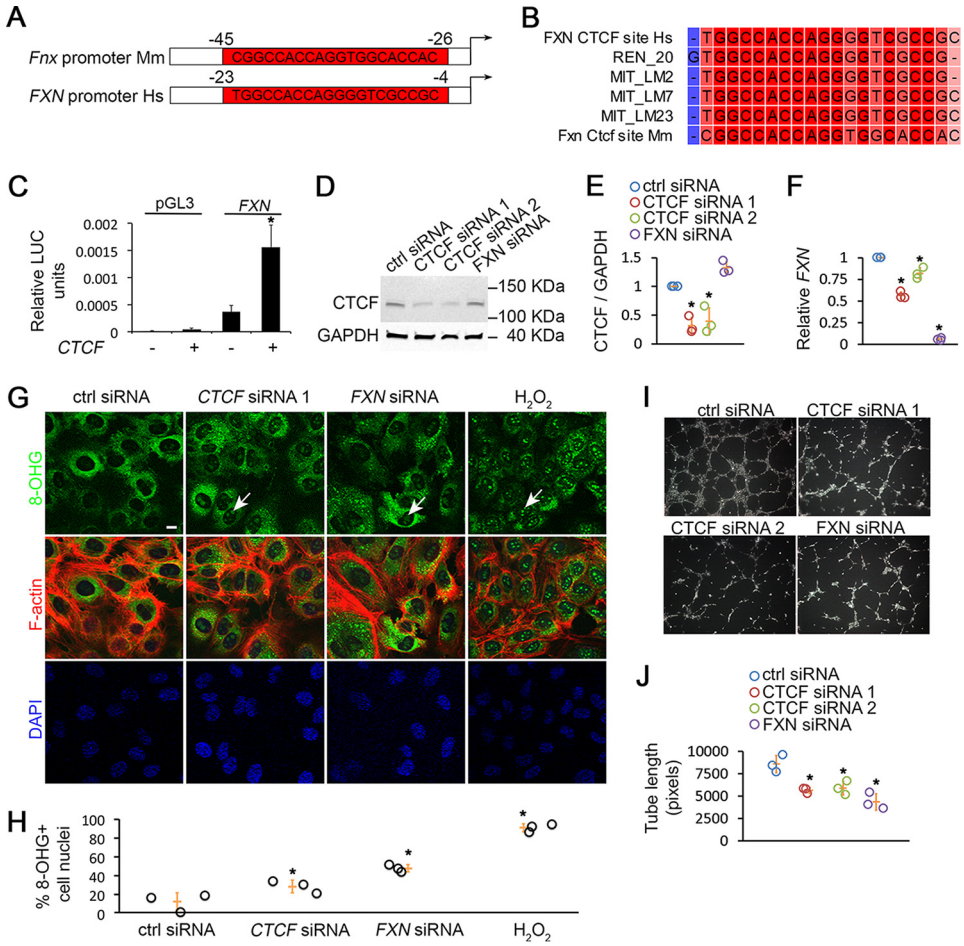

Figure 5. Ctcf activates the Fxn promoter, limits ROS accumulation, and promotes angiogenesis *in vitro*. *A*, scheme showing location of a Ctcf-binding site in the mouse (*Mm*) and human (*Hs*) *FXN* promoter relative to the transcription start site (*arrow*). *B*, alignment of the Ctcf-binding site in the mouse (Fxn Ctcf site Mm) and human (FXN CTCF site Hs) *FXN* promoter, with validated Ctcf-binding sites REN_20, MIT_LM2, MIT_LM7, and MIT_LM23. *C*, Luciferase activity normalized to Renilla activity of a control reporter (*pGL3*) or a *FXN* reporter cotransfected into BAECs with an empty (−) vector or a CTCF overexpression vector. *Error bars* represent the mean ± S.D. of a representative experiment of four performed with three technical replicates each. *, $p < 0.05$. *D*, Western blotting for CTCF in lysates of cells transfected with a negative control, two nonoverlapping anti-CTCF or anti-FXN siRNAs. GAPDH was used as loading control. *E*, densitometric quantification of Western blots from *D*. Data shown are CTCF normalized to GAPDH ± S.E., of three biological replicates. *, $p < 0.05$ compared with negative control (*crtl*). *F*, expression of *FXN* mRNA in HUVEC transfected with negative control, anti-CTCF, or anti-FXN siRNAs. Data shown are mean relative expression ± S.D. of three biological replicates. *, $p < 0.05$. *G*, immunofluorescence for 8-OHG and F-actin on HUVECs transfected with control (*ctrl*), anti-CTCF, or FXN siRNAs or treated with 200 μM H_2O_2. Nuclei were counterstained with DAPI. *Scale bar* = 10 μm. *H*, quantification of 8-OHG–positive nuclei in HUVECs transfected with control (*ctrl*), anti-CTCF, or FXN siRNAs or treated with 200 μM H_2O_2. *Error bars* represent the mean ± S.D. of three biological replicates. *, $p < 0.05$. *I*, fluorescent images of Matrigel tube formation assay from HUVEC transfected with negative control, anti-CTCF, or anti-FXN siRNA. *J*, total tube length calculated from images in *I*. Data shown are average tube length of three biological replicates ± S.E. *, $p < 0.05$ compared with negative control.

surrounding enhancers from activating its expression (15, 63). Accordingly, depletion of Ctcf by shRNA injection in the subretinal space causes excess intraretinal vascularization (15). In contrast, we found that *Ctcf* inactivation in endothelial cells negatively affects embryonic vascular development, and that *Vegf* expression was not altered in *Ctcf* mutant endothelial cells in our RNA-Seq and qPCR analysis (Fig. S6). This suggests alternative or context-specific functions for Ctcf in developing vascular endothelium. We found that Ctcf limits oxidative stress in endothelial cells. ROS modulate key signaling pathways controlling vascular development during embryogenesis and regenerative processes (64). Moderate oxidative stress and ROS levels can favor, whereas excessive oxidative stress can be detrimental to, vascular development (51, 65). Our results suggest that Ctcf is an important modulator of oxidative stress that prevents excessive ROS accumulation in endothelial cells to promote vascular development.

Ctcf is known to affect the proliferation and survival of particular cell types. For example, Ctcf promotes T cell proliferation in the thymus (37). In contrast, Ctcf deficiency in the developing limb or heart does not affect mesenchyme cell (9) or cardiomyocyte (14) proliferation, however, it induces mesenchyme cell apoptosis (9). We found that Ctcf deficiency does not affect proliferation nor does it induce apoptosis in embryonic endothelial cells, suggesting that Ctcf regulates cell growth and maintenance cell specifically. Proliferating endothelial cells produce higher ROS levels than quiescent cells (66). ROS induces activation of signaling pathways that promote endothelial cell proliferation and survival (67). It is possible that increased ROS production might have prevented imbalanced proliferation and apoptosis in Ctcf-depleted endothelial cells at least before E10.5. Alternatively, other mechanisms of cell death, including ferroptosis, might have been affected in *Ctcf* mutants. Ferroptosis is an iron-regulated route of cell death (68,

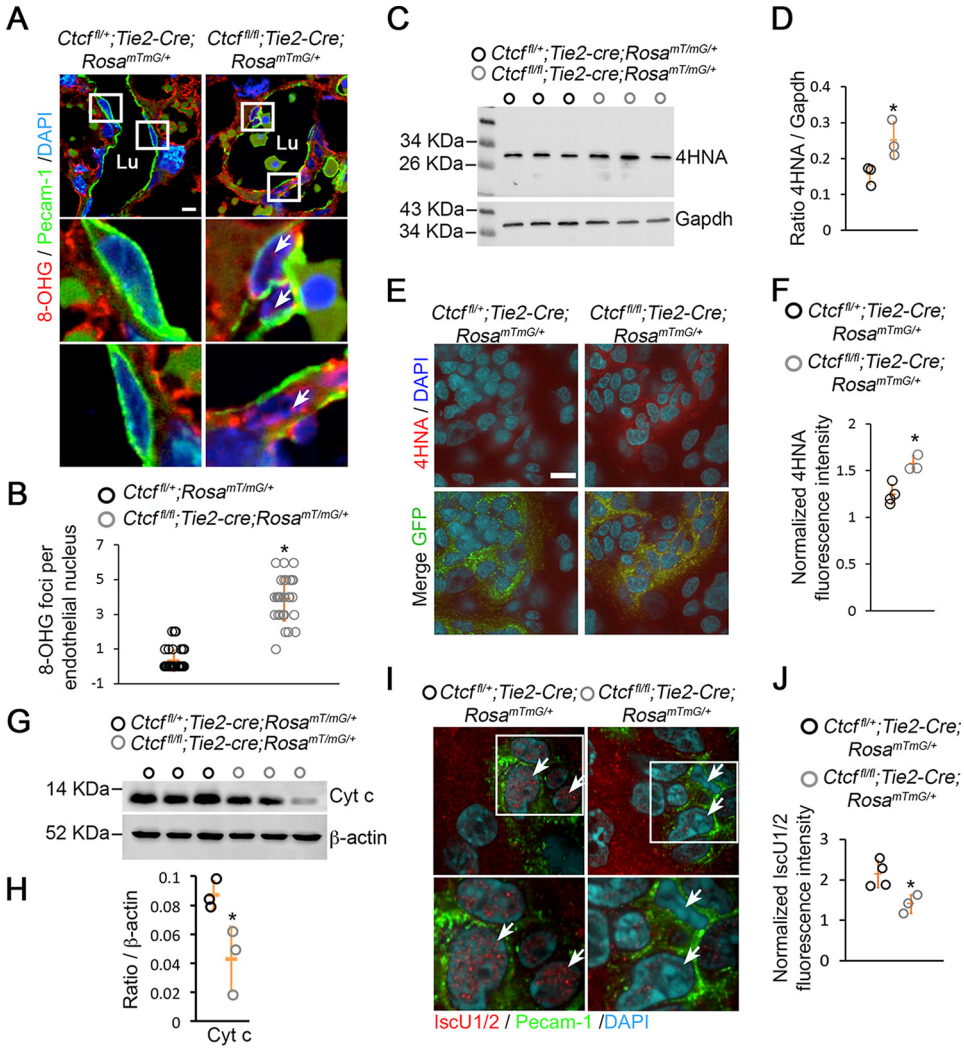

Figure 6. Ctcf limits ROS in endothelial cells *in vivo*. *A*, immunofluorescence for 8-OHG and Pecam-1 on sections of control (*Ctcf*$^{fl/+}$*;Tie2-cre;Rosa*$^{mT/mG/+}$) and *Ctcf* mutant (*Ctcf*$^{fl/fl}$*;Tie2-cre;Rosa*$^{mT/mG/+}$) placentae at E9.5. *Boxes* locate close-ups in *lower panels*. *Arrows* point to 8-OHG–positive endothelial cell nuclei in *Ctcf* mutant placentae. *Scale bar* = 10 μm. *B*, count of 8-OHG foci per nucleus of endothelial cells in control and *Ctcf* mutant placentae. *Error bars* represent the mean ± S.D. of cells quantified in three embryos. *, $p < 0.05$. *C*, Western blotting of 4HNA on control and *Ctcf* mutant labyrinths at E9.5. Gapdh was used a loading control. *D*, quantification of 4HNA relative to Gapdh from blot in *C*. *Error bars* represent the mean ± S.D. of three labyrinths. *, $p < 0.05$. *E*, immunofluorescence for 4HNA on E9.5 control and mutant placentae. Endothelial cells are revealed by staining for GFP. Nuclei were counterstained with DAPI. *Scale bar* = 10 μm. *F*, fluorescence for 4HNA in control and mutant E9.5 placentae normalized against fluorescence in the cytoplasmic region of Pecam-1 negative cells. *G*, Western blotting for cytochrome *c* (*Cyt c*), on labyrinth tissue from control and *Ctcf* mutant placentae at E9.5. B-actin was used as loading control. *H*, protein quantification relative to B-actin from blots in *G*. *Error bars* represent the mean ± S.D. of three biological replicates. *, $p < 0.05$. *I*, immunofluorescence for IscU1/2 and Pecam-1 on sections of control and mutant placentae at E9.5. *Arrows* point to nuclei. *Boxes* are close-ups in *lower panels*. *J*, fluorescence of IscU1/2 in control and mutant E9.5 placentae normalized against fluorescence in nuclei in Pecam-1 negative cells. *Error bars* represent the mean ± S.D. of three and four labyrinths. *, $p < 0.05$.

69) dependent on fatty acid synthesis and cysteine transport (70). These processes are linked to 4HNA (70), which was increased in *Ctcf* mutant placentae (Fig. 6, *C–F*). To the best of our knowledge, our work demonstrates for the first time that Ctcf regulates ROS accumulation. Future experiments will be required to directly test the extent to which Frataxin is responsible for the oxidative phenotype in *Ctcf* knockdown endothelial cells. If Ctcf regulates ROS levels in other cell types, it will be of interest to determine whether sensitivity to different ROS levels underlies cell-specific functions of Ctcf.

Decreased ability of cells to relieve oxidative stress has been implicated in cancer, diabetes, and aging and in neurodegenerative (71) and cardiovascular pathogenesis (51, 72). Neurons and cerebellar granule cells from a mouse model of FRDA generate ROS, resulting in decreased GSH (55). In addition, models of frataxin deficiency in yeast, fly, mouse, and cells in culture (73) support a function for frataxin in preventing ROS-induced toxicity in FRDA pathology (74, 75). Accordingly, reducing ROS prevents early mortality in frataxin-deficient *Drosophila* (76), and improves electrical contraction, coupling, and decay velocity of calcium kinetics in cardiomyocytes derived from stem cells from FRDA patients (77). Endothelial dysfunction has been associated with FRDA (27). However, how oxidative stress in endothelial cells contributes to FRDA has not been investigated. Our finding of decreased frataxin and increased ROS in Ctcf-deficient endothelial cells opens the possibility to investigate the endothelial component of FRDA.

Oxidative stress can potentially alter global gene expression patterns (78). We found that Ctcf-depleted developing endothelial cells are under oxidative stress and misregulate hundreds of genes. It will be of interest to determine whether Ctcf depletion alters interaction of distal regulatory elements resulting in dysregulated oxidative stress responses in endothelial cells during development. Our results indicate that Ctcf is an important regulator of oxidative stress in developing endothelial cells and open the possibility to investigate the endothelial component of diseases associated with oxidative stress.

Experimental procedures

Mice

All animal procedures were approved by the Animal Care Committee at the Hospital for Sick Children and followed the guidelines of The Centre for Phenogenomics. The following strains were used: $Ctcf^{fl/fl}$ (37), *Tie2-cre* (38), and $ROSA26^{mT/mG}$ (44). Presence of vaginal plugs indicated E0.5. Embryos not carrying the $ROSA26^{mT/mG}$ transgene were obtained by crossing $Ctcf^{fl/+}$; *Tie2-cre* males with $Ctcf^{fl/fl}$ females. Embryos carrying the $ROSA26^{mT/mG}$ transgene were obtained by crossing $Ctcf^{fl/+}$;*Tie2-cre* males with $Ctcf^{fl/fl}$;$ROSA26^{mT/mG/mT/mG}$ females.

Genotyping

Tail clips, ear notches, and yolk sacs were digested in 300 μl of 50 mM NaOH at 95 °C for 10–30 min, and 100 μl of 0.5 μm Tris-HCl were added to neutralize the reaction (79). 1 μl of the digestion was used for PCR. Amplification conditions used to identify floxed *Ctcf* alleles were the following: 94 °C 3 min, 94 °C 30 s, 63 °C 30 s, 72 °C for 1 min, steps 2–4 for 35 cycles, and 72 °C for 5 min. Amplification conditions used for *Cre* were the following: 95 °C 2 min, 95 °C 40 s, 55 °C 50 s, 72 °C 1 min, steps 2–4 for 35 cycles, and 72 °C for 10 min. Primers are in Table S1.

Fixation and histology

Freshly dissected embryos in cold PBS were fixed in 4% paraformaldehyde (PFA) overnight at 4 °C. Tissues were washed twice in PBS for 30 min at 4 °C and stored in 70% ethanol overnight at 4 °C. Tissues were washed in the following ethanol and xylene series at room temperature: 85% EtOH for 30 min twice, 95% EtOH for 30 min twice, 100% EtOH for 45 min four times, 100% xylene for 5 min, and 100% xylene for 10 min three times. Tissues were incubated in 50% xylene:wax at 60 °C for 30 min and stored at room temperature overnight. The next day, tissues were incubated at 60 °C for 30 min, washed with 100% wax for 1 h at 60 °C twice, and after refreshing the wax, incubated for 2 h at 60 °C. Tissues were then embedded in wax blocks that were mounted on histology cassettes. 4- to 8-μm-thick sections were generated, mounted on glass slides, and stained with hematoxylin and eosin as follows. Slides were washed in xylene for 10 min twice, 100% EtOH for 2 min twice, 90% EtOH for 2 min, 70% EtOH for 2 min, 50% for 2 min, 30% for 2 min, and quickly washed with tap water three times. Slides were stained with 100% hematoxylin for 10 min, quickly washed three times with tap water, placed in 0.5% acid alcohol for 5 s, quickly washed three times with tap water, placed in 1% lithium carbonate for 5 s, washed with tap water three times, 30% EtOH, 50% EtOH, and 70% EtOH for 1min. Slides were then stained in 3% eosin for 10 min, washed in 90% EtOH for 1 min, 100% EtOH twice for 1 min, and placed in xylene twice for 5min. Slides were mounted with Permount (Fisher).

Immunofluorescence and whole mount immunostaining

Dissected tissues were fixed in 4% PFA overnight at 4 °C, washed in PBS three times for 10 min at room temperature, and kept in 30% sucrose/PBS at 4 °C overnight or until tissues sank down. Tissues were embedded in OCT compound and sectioned. 4-μm frozen sections were mounted on glass slides, fixed in 4% PFA for 5 min, and washed in PBS three times, 5 min each. Slides were blocked with 5% goat serum, 0.1% Triton X-100 in PBS for 15 min and incubated with primary antibodies overnight at 4 °C in a humidified chamber. Slides were washed in PBS three times for 10 min each, incubated with secondary antibodies diluted in blocking buffer for 1 h at room temperature. Slides were washed in PBS three times 5 min each and PBS with 0.05% Tween 20 for 5 min. Slides were mounted in Vectashield Mounting Medium with DAPI (Vector Laboratories). Antibodies and dilutions were as follows: Ctcf (1/300) (80) (Santa Cruz Biotechnology, G-8), phosphorylated histone H3 (1:100) (Santa Cruz, SC-8656-R), cleaved caspase 3 (1:100) (Cell Signaling Technologies, 9661), CT3 (1:200) (Development Studies Hybridoma Bank), CD31/Pecam-1 (1:100) (BD Pharmingen, 553370), IscU1/2 (1:1000) (Santa Cruz Biotechnology, sc-373694), and GFP (1:1000) (GeneScript, A01694).

Embryos for whole mount immunostaining were fixed in 4% PFA overnight and washed three times in PBS for 5 min each. Embryos were permeabilized and blocked for 1 h at room temperature in PBT (1× PBS with 0.2% Triton X-100) with 0.1% BSA and 2% goat serum. Embryos were incubated in anti–Pecam-1 antibody diluted in blocking buffer (0.1% BSA and 2% normal goat serum) overnight at 4 °C. Samples were washed five times for 5 min with PBS, blocked in PBT with 2% normal goat serum for 1 h at room temperature, and incubated with secondary antibodies, diluted in 0.15 BSA and 2% goat serum, for 1 h in the dark at room temperature. Samples were washed five times for 5 min each with PBS and cleared in 1:1 glycerol: PBS for 3 h at 4 °C, and then in 80% glycerol:PBS for 1 h at 4 °C before imaging (81).

Cells were transfected at 50% confluence on 10 μg/ml fibronectin-coated Permanox 8-well chamber slides (Thermo Fisher) and allowed to grow to confluence. Cells were then fixed with 4% paraformaldehyde for 20 min, followed by permeabilization for 5 min with 0.2% Triton X-100, and blocking with 5% BSA/PBST for 1 h. Cells were then incubated with mouse anti–8-hydroxyguanosine (1:100) (Santa Cruz Biotechnology), followed by incubation with rabbit anti-mouse IgG 488 (1:200) (Invitrogen), and counterstained and mounted in Vectashield Mounting Medium with DAPI (Vector Laboratories). For actin staining, after incubation with secondary antibody, cells were washed and incubated with rhodamine-phalloidin (1:40) (Invitrogen) for 30 min at room temperature. Images were taken on an Olympus FV1000 Confocal microscope

using a LumPlanFI40X/0.8NA objective. The total number of nuclei was divided by the number of nuclei that had an 8-OHG signal.

Gene expression analysis

GFP-positive cells were sorted from control *Ctcf*$^{fl/+}$*;Tie2-cre;Rosa*$^{mT/mG}$ and mutant *Ctcf*$^{fl/fl}$*;Tie2-cre;Rosa*$^{mT/mG}$ yolk sacs and placentae, and RNA was isolated using the Direct-zol™ RNA Miniprep kit (Zymo Research). cDNA was synthesized using the SuperScript® VILO cDNA synthesis kit (Thermo Fisher Scientific). cDNA was used in qPCR done using SsoAdvanced™ Universal SYBR® Green Supermix (Bio-Rad) on a CFX384 Touch™ Real-Time PCR Detection System (Bio-Rad). Data were analyzed using CFX Manager Software (Bio-Rad) and normalized to *Pgk1* expression levels. qPCR primer sequences are in Table S1.

RNA-seq

Endothelial cell RNA was isolated from GFP-positive cells (82, 83) sorted from individual dissected placental labyrinth (84) of control *Ctcf*$^{fl/+}$*;Tie2-cre;Rosa*$^{mT/mG}$ and mutant *Ctcf*$^{fl/fl}$*;Tie2-cre;Rosa*$^{mT/mG}$ embryos using Direct-zol™ RNA Miniprep Plus Kit (Zymo Research) and treated with DNase according to the manufacturer's protocol. RNA integrity was verified using the Agilent Bioanalyzer (Agilent Technologies). Three biological replicates were used for each group. RNA-Seq libraries were prepared using the Ovation® Single Cell RNA-Seq System (NuGEN Technologies) and sequenced in single-end sequence reads (50 bp in length) on the Illumina HiSeq 2500 platform. The first 8-bp sequences of the 5′ end of the sequencing reads were trimmed using Trimmomatic (85), as recommended by the Ovation® Single Cell RNA-Seq System (NuGEN) protocol. Trimmed high-quality reads were then mapped to the mouse genome (mm10) using STAR v2.4.2a (86). Mapped read counts were obtained using HTseq (87). Differential expression analysis and MA plots was performed using DESeq2 (88). Enrichment of gene ontology categories in differentially expressed genes was determined using DAVID (89).

Cell culture and transfection

HUVEC and BAEC (ScienCell Research Laboratories) were cultured in Endothelial Cell Medium (ScienCell), 5% fetal bovine serum (FBS), 1% endothelial cell growth supplement (ScienCell), and 1% penicillin/streptomycin. Cells were grown on attachment factor (Gibco)–coated culture dishes and used from passage 3 to passage 6 in experiments. BAECs (Lonza) were cultured in DMEM high glucose (Gibco) with 10% FBS, and 1% penicillin/streptomycin. HUVEC were transfected with 40 nM siRNA using RNAi Max (Invitrogen) per manufacturer's instructions. After 48 h, knockdown was confirmed via qRT-PCR and/or Western blotting.

Tube formation assay

Matrigel (Corning) was polymerized in μ-Slide Angiogenesis chambers (ibidi) for 1 h at 37 °C. siRNA transfected HUVECs were incubated with 5 μM Cell Tracker Green (Thermo Fisher) for 30 min at 37 °C and seeded onto Matrigel for 8 h. Images were taken on a stereo microscope (Leica M165FC), and total tube length was calculated using angiogenesis analyzer (ImageJ). Two fields of view were analyzed per condition and averaged each experiment.

siRNA and plasmids

Nontargeting *Silencer* Select Negative Control No. 1 siRNA, *CTCF* siRNA No. 1 and siRNA No. 2 (assay IDs: s20967 and s3855), and *Frataxin* siRNA (assay ID: s5360) were from Ambion/Invitrogen. The luciferase reporter was constructed by cloning a 386-bp PCR product corresponding to the *Frataxin* promoter into pGL3 Basic. Primers are in Table S1. The CTCF overexpression plasmid PCI-7.1 was described previously.

Luciferase assays

Confluent BAECs were transfected with 0.5 μg of *FXN* luciferase construct, 0.5 μg of human CTCF overexpression construct, and 0.1 μg of pRenilla construct using Lipofectamine 2000 (2 μl) in Opti-MEM (Invitrogen). Transfection was performed in 12-well dishes and media were changed back to Endothelial Cell Medium after 5 h. After 24 h, dual luciferase (*Renilla* and Firefly) was measured using a GloMax 20/20 Luminometer (Promega) using the Dual-Luciferase Reporter Assay System (Promega).

Western blotting

siRNA transfected cells were lysed in 2× Laemelli buffer and boiled at 95 °C for 10 min and centrifuged. Samples were then loaded on precast SDS-PAGE gels (Bio-Rad) for Western blot analysis. Antibodies used were CTCF (1:500) (Santa Cruz Biotechnology, sc-271474), GAPDH (1:5000) (Santa Cruz Biotechnology, sc-47724), 4 hydroxynonenal (1:200) (Abcam, ab46545), Frataxin (1:100) (Abcam, 175402), cytochrome *c* (1:1000) (Santa Cruz Biotechnology, sc-13156), IscU1/2 (1:1000) (Santa Cruz Biotechnology, sc-373694), and HRP-conjugated goat anti-mouse IgG (1:3000) (Cell Signaling Technology, 7076). Blots were processed using MicroChemi 4.2 (DNR Bio-Imaging Systems).

Microscopy and imaging

Nikon SMZ1500 and Nikon Eclipse Ni microscopes were used. Images were analyzed and quantified using ImageJ Cell Counter and Angiogenic Analyzer tools.

Statistical analysis

Data are presented as the mean ± S.D. or S.E., as indicated. Data were compared by Student's *t* test. $p < 0.5$ was considered significant. At least three biological replicates were compared in all analyses.

Author contributions—A. R. R. designed and performed experiments, analyzed data, and wrote the manuscript with P. D. O., A. A., L. C., P. V. D., and N. K. designed and performed experiments and analyzed data. J. E. F. designed experiments, analyzed data, and edited the manuscript. M. D. W. analyzed data. N. G. provided the *Ctcf*$^{fl/fl}$ mouse line and P. D. O. conceived the study, designed and performed experiments, analyzed data, and wrote the manuscript with A. R. R with input from all authors.

Acknowledgments—We thank Meaghan Leslie for help with qPCR, Félix Recillas-Targa (Universidad Nacional Autónoma de México) for kindly providing the anti-Ctcf antibody, Sergio Pereira (The Centre for Applied Genomics) for next generation sequencing, Sheyun Zhao (SickKids-UHN Flow Cytometry Facility) for help with cell sorting, Laura Caporiccio for mouse colony management, and The Centre for Phenogenomics (TCP) for mouse husbandry and care.

References

1. Phillips, J. E., and Corces, V. G. (2009) CTCF: Master weaver of the genome. *Cell* **137,** 1194–1211 CrossRef Medline
2. Battistelli, C., Busanello, A., and Maione, R. (2014) Functional interplay between MyoD and CTCF in regulating long-range chromatin interactions during differentiation. *J. Cell Sci.* **127,** 3757–3767 CrossRef Medline
3. Delgado-Olguín, P., Brand-Arzamendi, K., Scott, I. C., Jungblut, B., Stainier, D. Y., Bruneau, B. G., and Recillas-Targa, F. (2011) CTCF promotes muscle differentiation by modulating the activity of myogenic regulatory factors. *J. Biol. Chem.* **286,** 12483–12494 CrossRef Medline
4. Göndör, A., and Ohlsson, R. (2009) Chromosome crosstalk in three dimensions. *Nature* **461,** 212–217 CrossRef Medline
5. Busslinger, G. A., Stocsits, R. R., van der Lelij, P., Axelsson, E., Tedeschi, A., Galjart, N., and Peters, J. M. (2017) Cohesin is positioned in mammalian genomes by transcription, CTCF and Wapl. *Nature* **544,** 503–507 CrossRef Medline
6. Lupiáñez, D. G., Kraft, K., Heinrich, V., Krawitz, P., Brancati, F., Klopocki, E., Horn, D., Kayserili, H., Opitz, J. M., Laxova, R., Santos-Simarro, F., Gilbert-Dussardier, B., Wittler, L., Borschiwer, M., Haas, S. A., *et al.* (2015) Disruptions of topological chromatin domains cause pathogenic rewiring of gene-enhancer interactions. *Cell* **161,** 1012–1025 CrossRef Medline
7. Narendra, V., Bulajić, M., Dekker, J., Mazzoni, E. O., and Reinberg, D. (2016) CTCF-mediated topological boundaries during development foster appropriate gene regulation. *Genes Dev.* **30,** 2657–2662 CrossRef Medline
8. Moore, J. M., Rabaia, N. A., Smith, L. E., Fagerlie, S., Gurley, K., Loukinov, D., Disteche, C. M., Collins, S. J., Kemp, C. J., Lobanenkov, V. V., and Filippova, G. N. (2012) Loss of maternal CTCF is associated with peri-implantation lethality of Ctcf null embryos. *PloS One* **7,** e34915 CrossRef Medline
9. Soshnikova, N., Montavon, T., Leleu, M., Galjart, N., and Duboule, D. (2010) Functional analysis of CTCF during mammalian limb development. *Dev. Cell* **19,** 819–830 CrossRef Medline
10. Li, T., Lu, Z., and Lu, L. (2004) Regulation of eye development by transcription control of CCCTC binding factor (CTCF). *J. Biol. Chem.* **279,** 27575–27583 CrossRef Medline
11. Herold, M., Bartkuhn, M., and Renkawitz, R. (2012) CTCF: Insights into insulator function during development. *Development* **139,** 1045–1057 CrossRef Medline
12. Wan, L. B., Pan, H., Hannenhalli, S., Cheng, Y., Ma, J., Fedoriw, A., Lobanenkov, V., Latham, K. E., Schultz, R. M., and Bartolomei, M. S. (2008) Maternal depletion of CTCF reveals multiple functions during oocyte and preimplantation embryo development. *Development* **135,** 2729–2738 CrossRef Medline
13. Hirayama, T., Tarusawa, E., Yoshimura, Y., Galjart, N., and Yagi, T. (2012) CTCF is required for neural development and stochastic expression of clustered Pcdh genes in neurons. *Cell Rep.* **2,** 345–357 CrossRef Medline
14. Gomez-Velazquez, M., Badia-Careaga, C., Lechuga-Vieco, A. V., Nieto-Arellano, R., Tena, J. J., Rollan, I., Alvarez, A., Torroja, C., Caceres, E. F., Roy, A. R., Galjart, N., Delgado-Olguin, P., Sanchez-Cabo, F., Enriquez, J. A., Gomez-Skarmeta, J. L., and Manzanares, M. (2017) CTCF counter-regulates cardiomyocyte development and maturation programs in the embryonic heart. *PLoS Genetics* **13,** e1006985 CrossRef Medline
15. Tang, M., Chen, B., Lin, T., Li, Z., Pardo, C., Pampo, C., Chen, J., Lien, C. L., Wu, L., Ai, L., Wang, H., Yao, K., Oh, S. P., Seto, E., Smith, L. E., Siemann, D. W., Kladde, M. P., Cepko, C. L., and Lu, J. (2011) Restraint of angiogenesis by zinc finger transcription factor CTCF-dependent chromatin insulation. *Proc. Natl. Acad. Sci. U.S.A.* **108,** 15231–15236 CrossRef Medline
16. Garcia, M. D., and Larina, I. V. (2014) Vascular development and hemodynamic force in the mouse yolk sac. *Front. Physiol.* **5,** 308 CrossRef Medline
17. Watson, E. D., and Cross, J. C. (2005) Development of structures and transport functions in the mouse placenta. *Physiology (Bethesda)* **20,** 180–193 CrossRef Medline
18. Olsson, A. K., Dimberg, A., Kreuger, J., and Claesson-Welsh, L. (2006) VEGF receptor signaling—in control of vascular function. *Nat. Rev. Mol. Cell Biol.* **7,** 359–371 CrossRef Medline
19. De Val, S., and Black, B. L. (2009) Transcriptional control of endothelial cell development. *Dev. Cell* **16,** 180–195 CrossRef Medline
20. Coultas, L., Chawengsaksophak, K., and Rossant, J. (2005) Endothelial cells and VEGF in vascular development. *Nature* **438,** 937–945 CrossRef Medline
21. Fish, J. E., and Wythe, J. D. (2015) The molecular regulation of arteriovenous specification and maintenance. *Dev. Dyn.* **244,** 391–409 CrossRef Medline
22. Demicheva, E., and Crispi, F. (2014) Long-term follow-up of intrauterine growth restriction: Cardiovascular disorders. *Fetal Diagn. Ther.* **36,** 143–153 CrossRef Medline
23. Shaut, C. A., Keene, D. R., Sorensen, L. K., Li, D. Y., and Stadler, H. S. (2008) HOXA13 is essential for placental vascular patterning and labyrinth endothelial specification. *PLoS Genetics* **4,** e1000073 CrossRef Medline
24. Santos, R., Lefevre, S., Sliwa, D., Seguin, A., Camadro, J. M., and Lesuisse, E. (2010) Friedreich ataxia: Molecular mechanisms, redox considerations, and therapeutic opportunities. *Antioxid. Redox Signal.* **13,** 651–690 CrossRef Medline
25. Nachbauer, W., Boesch, S., Reindl, M., Eigentler, A., Hufler, K., Poewe, W., Löscher, W., and Wanschitz, J. (2012) Skeletal muscle involvement in Friedreich ataxia and potential effects of recombinant human erythropoietin administration on muscle regeneration and neovascularization. *J. Neuropathol. Exp. Neurol.* **71,** 708–715 CrossRef Medline
26. Raman, S. V., Phatak, K., Hoyle, J. C., Pennell, M. L., McCarthy, B., Tran, T., Prior, T. W., Olesik, J. W., Lutton, A., Rankin, C., Kissel, J. T., and Al-Dahhak, R. (2011) Impaired myocardial perfusion reserve and fibrosis in Friedreich ataxia: A mitochondrial cardiomyopathy with metabolic syndrome. *Eur. Heart J.* **32,** 561–567 CrossRef Medline
27. Siasos, G., Gialafos, E., Tousoulis, D., Oikonomou, E., Michalea, S., Kollia, C., Aggeli, C., Maniatis, K., Paraskevopoulos, T., Zisimos, K., Kioufis, S., Papavassiliou, A. G., and Stefanadis, C. (2011) Friedreich ataxia is associated with endothelial dysfunction and increased arterial stiffness. *Circulation* **124,** Suppl. 21, Abstract 9993
28. Patel, P. I., and Isaya, G. (2001) Friedreich ataxia: From GAA triplet-repeat expansion to frataxin deficiency. *Am. J. Hum. Genet.* **69,** 15–24 CrossRef Medline
29. Gakh, O., Park, S., Liu, G., Macomber, L., Imlay, J. A., Ferreira, G. C., and Isaya, G. (2006) Mitochondrial iron detoxification is a primary function of frataxin that limits oxidative damage and preserves cell longevity. *Hum. Mol. Genet.* **15,** 467–479 CrossRef Medline
30. Schulz, J. B., Dehmer, T., Schöls, L., Mende, H., Hardt, C., Vorgerd, M., Bürk, K., Matson, W., Dichgans, J., Beal, M. F., and Bogdanov, M. B. (2000) Oxidative stress in patients with Friedreich ataxia. *Neurology* **55,** 1719–1721 CrossRef Medline
31. Pandey, A., Gordon, D. M., Pain, J., Stemmler, T. L., Dancis, A., and Pain, D. (2013) Frataxin directly stimulates mitochondrial cysteine desulfurase by exposing substrate-binding sites, and a mutant Fe-S cluster scaffold protein with frataxin-bypassing ability acts similarly. *J. Biol. Chem.* **288,** 36773–36786 CrossRef Medline
32. Koutnikova, H., Campuzano, V., Foury, F., Dollé, P., Cazzalini, O., and Koenig, M. (1997) Studies of human, mouse and yeast homologues indicate a mitochondrial function for frataxin. *Nat. Genet.* **16,** 345–351 CrossRef Medline
33. Gottesfeld, J. M., Rusche, J. R., and Pandolfo, M. (2013) Increasing frataxin gene expression with histone deacetylase inhibitors as a therapeutic ap-

proach for Friedreich's ataxia. *J. Neurochem.* **126,** Suppl. 1, 147–154 CrossRef Medline
34. Rai, M., Soragni, E., Jenssen, K., Burnett, R., Herman, D., Coppola, G., Geschwind, D. H., Gottesfeld, J. M., and Pandolfo, M. (2008) HDAC inhibitors correct frataxin deficiency in a Friedreich ataxia mouse model. *PloS One* **3,** e1958 CrossRef Medline
35. Herman, D., Jenssen, K., Burnett, R., Soragni, E., Perlman, S. L., and Gottesfeld, J. M. (2006) Histone deacetylase inhibitors reverse gene silencing in Friedreich's ataxia. *Nat. Chem. Biol.* **2,** 551–558 CrossRef Medline
36. Sandi, C., Pinto, R. M., Al-Mahdawi, S., Ezzatizadeh, V., Barnes, G., Jones, S., Rusche, J. R., Gottesfeld, J. M., and Pook, M. A. (2011) Prolonged treatment with pimelic *o*-aminobenzamide HDAC inhibitors ameliorates the disease phenotype of a Friedreich ataxia mouse model. *Neurobiol. Dis.* **42,** 496–505 CrossRef Medline
37. Heath, H., Ribeiro de Almeida, C., Sleutels, F., Dingjan, G., van de Nobelen, S., Jonkers, I., Ling, K. W., Gribnau, J., Renkawitz, R., Grosveld, F., Hendriks, R. W., and Galjart, N. (2008) CTCF regulates cell cycle progression of $\alpha\beta$ T cells in the thymus. *EMBO J.* **27,** 2839–2850 CrossRef Medline
38. Proctor, J. M., Zang, K., Wang, D., Wang, R., and Reichardt, L. F. (2005) Vascular development of the brain requires beta8 integrin expression in the neuroepithelium. *J. Neurosci.* **25,** 9940–9948 CrossRef Medline
39. Sohn, S. J., Sarvis, B. K., Cado, D., and Winoto, A. (2002) ERK5 MAPK regulates embryonic angiogenesis and acts as a hypoxia-sensitive repressor of vascular endothelial growth factor expression. *J. Biol. Chem.* **277,** 43344–43351 CrossRef Medline
40. Maltepe, E., Schmidt, J. V., Baunoch, D., Bradfield, C. A., and Simon, M. C. (1997) Abnormal angiogenesis and responses to glucose and oxygen deprivation in mice lacking the protein ARNT. *Nature* **386,** 403–407 CrossRef Medline
41. Zudaire, E., Gambardella, L., Kurcz, C., and Vermeren, S. (2011) A computational tool for quantitative analysis of vascular networks. *PloS One* **6,** e27385 CrossRef Medline
42. Lucitti, J. L., Jones, E. A., Huang, C., Chen, J., Fraser, S. E., and Dickinson, M. E. (2007) Vascular remodeling of the mouse yolk sac requires hemodynamic force. *Development* **134,** 3317–3326 CrossRef Medline
43. Cross, J. C. (2005) How to make a placenta: Mechanisms of trophoblast cell differentiation in mice–a review. *Placenta* **26,** Suppl. A, S3–S9 CrossRef Medline
44. Muzumdar, M. D., Tasic, B., Miyamichi, K., Li, L., and Luo, L. (2007) A global double-fluorescent Cre reporter mouse. *Genesis* **45,** 593–605 CrossRef Medline
45. Chutake, Y. K., Costello, W. N., Lam, C., and Bidichandani, S. I. (2014) Altered nucleosome positioning at the transcription start site and deficient transcriptional initiation in Friedreich ataxia. *J. Biol. Chem.* **289,** 15194–15202 CrossRef Medline
46. De Biase, I., Chutake, Y. K., Rindler, P. M., and Bidichandani, S. I. (2009) Epigenetic silencing in Friedreich ataxia is associated with depletion of CTCF (CCCTC-binding factor) and antisense transcription. *PloS One* **4,** e7914 CrossRef Medline
47. Yandim, C., Natisvili, T., and Festenstein, R. (2013) Gene regulation and epigenetics in Friedreich's ataxia. *J. Neurochem.* **126,** Suppl. 1, 21–42 CrossRef Medline
48. Ziebarth, J. D., Bhattacharya, A., and Cui, Y. (2013) CTCFBSDB 2.0: A database for CTCF-binding sites and genome organization. *Nucleic Acids Res.* **41,** D188–D194 CrossRef Medline
49. Bao, L., Zhou, M., and Cui, Y. (2008) CTCFBSDB: A CTCF-binding site database for characterization of vertebrate genomic insulators. *Nucleic Acids Res.* **36,** D83–D87 CrossRef Medline
50. Lefevre, S., Sliwa, D., Rustin, P., Camadro, J. M., and Santos, R. (2012) Oxidative stress induces mitochondrial fragmentation in frataxin-deficient cells. *Biochem. Biophys. Res. Commun.* **418,** 336–341 CrossRef Medline
51. Kim, Y. W., and Byzova, T. V. (2014) Oxidative stress in angiogenesis and vascular disease. *Blood* **123,** 625–631 CrossRef Medline
52. Armstrong, J. S., Steinauer, K. K., Hornung, B., Irish, J. M., Lecane, P., Birrell, G. W., Peehl, D. M., and Knox, S. J. (2002) Role of glutathione depletion and reactive oxygen species generation in apoptotic signaling in a human B lymphoma cell line. *Cell Death Differ.* **9,** 252–263 CrossRef Medline
53. Yan, H., Meng, F., Jia, H., Guo, X., and Xu, B. (2012) The identification and oxidative stress response of a zeta class glutathione S-transferase (GSTZ1) gene from *Apis cerana*. *J. Insect Physiol.* **58,** 782–791 CrossRef Medline
54. Nakada, Y., Canseco, D. C., Thet, S., Abdisalaam, S., Asaithamby, A., Santos, C. X., Shah, A. M., Zhang, H., Faber, J. E., Kinter, M. T., Szweda, L. I., Xing, C., Hu, Z., Deberardinis, R. J., Schiattarella, G., Hill, J. A., Oz, O., Lu, Z., Zhang, C. C., Kimura, W., and Sadek, H. A. (2017) Hypoxia induces heart regeneration in adult mice. *Nature* **541,** 222–227 CrossRef Medline
55. Abeti, R., Parkinson, M. H., Hargreaves, I. P., Angelova, P. R., Sandi, C., Pook, M. A., Giunti, P., and Abramov, A. Y. (2016) Mitochondrial energy imbalance and lipid peroxidation cause cell death in Friedreich's ataxia. *Cell Death Dis.* **7,** e2237 CrossRef Medline
56. Esterbauer, H., Schaur, R. J., and Zollner, H. (1991) Chemistry and biochemistry of 4-hydroxynonenal, malonaldehyde and related aldehydes. *Free Radic. Biol. Med.* **11,** 81–128 CrossRef Medline
57. Hüttemann, M., Pecina, P., Rainbolt, M., Sanderson, T. H., Kagan, V. E., Samavati, L., Doan, J. W., and Lee, I. (2011) The multiple functions of cytochrome *c* and their regulation in life and death decisions of the mammalian cell: From respiration to apoptosis. *Mitochondrion* **11,** 369–381 CrossRef Medline
58. Schoenfeld, R. A., Napoli, E., Wong, A., Zhan, S., Reutenauer, L., Morin, D., Buckpitt, A. R., Taroni, F., Lonnerdal, B., Ristow, M., Puccio, H., and Cortopassi, G. A. (2005) Frataxin deficiency alters heme pathway transcripts and decreases mitochondrial heme metabolites in mammalian cells. *Hum. Mol. Genet.* **14,** 3787–3799 CrossRef Medline
59. Lu, C., and Cortopassi, G. (2007) Frataxin knockdown causes loss of cytoplasmic iron-sulfur cluster functions, redox alterations and induction of heme transcripts. *Arch. Biochem. Biophys.* **457,** 111–122 CrossRef Medline
60. Tong, W. H., and Rouault, T. A. (2006) Functions of mitochondrial ISCU and cytosolic ISCU in mammalian iron-sulfur cluster biogenesis and iron homeostasis. *Cell Metab.* **3,** 199–210 CrossRef Medline
61. Martelli, A., Wattenhofer-Donzé, M., Schmucker, S., Bouvet, S., Reutenauer, L., and Puccio, H. (2007) Frataxin is essential for extramitochondrial Fe-S cluster proteins in mammalian tissues. *Hum. Mol. Genet.* **16,** 2651–2658 CrossRef Medline
62. Tong, W. H., and Rouault, T. (2000) Distinct iron-sulfur cluster assembly complexes exist in the cytosol and mitochondria of human cells. *EMBO J.* **19,** 5692–5700 CrossRef Medline
63. Lu, J., and Tang, M. (2012) CTCF-dependent chromatin insulator as a built-in attenuator of angiogenesis. *Transcription* **3,** 73–77 CrossRef Medline
64. Coant, N., Ben Mkaddem, S., Pedruzzi, E., Guichard, C., Tréton, X., Ducroc, R., Freund, J. N., Cazals-Hatem, D., Bouhnik, Y., Woerther, P. L., Skurnik, D., Grodet, A., Fay, M., Biard, D., Lesuffleur, T., *et al.* (2010) NADPH oxidase 1 modulates WNT and NOTCH1 signaling to control the fate of proliferative progenitor cells in the colon. *Mol. Cell. Biol.* **30,** 2636–2650 CrossRef Medline
65. Zhou, Y., Yan, H., Guo, M., Zhu, J., Xiao, Q., and Zhang, L. (2013) Reactive oxygen species in vascular formation and development. *Oxid. Med. Cell. Longev.* **2013,** 374963 CrossRef Medline
66. Peshavariya, H., Dusting, G. J., Jiang, F., Halmos, L. R., Sobey, C. G., Drummond, G. R., and Selemidis, S. (2009) NADPH oxidase isoform selective regulation of endothelial cell proliferation and survival. *Naunyn Schmiedebergs Arch. Pharmacol.* **380,** 193–204 CrossRef Medline
67. Petry, A., Djordjevic, T., Weitnauer, M., Kietzmann, T., Hess, J., and Görlach, A. (2006) NOX2 and NOX4 mediate proliferative response in endothelial cells. *Antioxid. Redox Signal.* **8,** 1473–1484 CrossRef Medline
68. Dixon, S. J., Lemberg, K. M., Lamprecht, M. R., Skouta, R., Zaitsev, E. M., Gleason, C. E., Patel, D. N., Bauer, A. J., Cantley, A. M., Yang, W. S., Morrison, B., 3rd, and Stockwell, B. R. (2012) Ferroptosis: An iron-dependent form of nonapoptotic cell death. *Cell* **149,** 1060–1072 CrossRef Medline
69. Dixon, S. J., and Stockwell, B. R. (2014) The role of iron and reactive oxygen species in cell death. *Nat. Chem. Biol.* **10,** 9–17 CrossRef Medline

70. Dalleau, S., Baradat, M., Guéraud, F., and Huc, L. (2013) Cell death and diseases related to oxidative stress: 4-hydroxynonenal (HNE) in the balance. *Cell Death Differ.* **20,** 1615–1630 CrossRef Medline
71. Lin, M. T., and Beal, M. F. (2006) Mitochondrial dysfunction and oxidative stress in neurodegenerative diseases. *Nature* **443,** 787–795 CrossRef Medline
72. Panth, N., Paudel, K. R., and Parajuli, K. (2016) Reactive oxygen species: A key hallmark of cardiovascular disease. *Adv. Med.* **2016,** 9152732 CrossRef Medline
73. Perdomini, M., Hick, A., Puccio, H., and Pook, M. A. (2013) Animal and cellular models of Friedreich ataxia. *J. Neurochem.* **126,** Suppl. 1, 65–79 CrossRef Medline
74. Park, S., Gakh, O., Mooney, S. M., and Isaya, G. (2002) The ferroxidase activity of yeast frataxin. *J. Biol. Chem.* **277,** 38589–38595 CrossRef Medline
75. O'Neill, H. A., Gakh, O., Park, S., Cui, J., Mooney, S. M., Sampson, M., Ferreira, G. C., and Isaya, G. (2005) Assembly of human frataxin is a mechanism for detoxifying redox-active iron. *Biochemistry* **44,** 537–545 CrossRef Medline
76. Anderson, P. R., Kirby, K., Orr, W. C., Hilliker, A. J., and Phillips, J. P. (2008) Hydrogen peroxide scavenging rescues frataxin deficiency in a *Drosophila* model of Friedreich's ataxia. *Proc. Natl. Acad. Sci. U.S.A.* **105,** 611–616 CrossRef Medline
77. Lee, Y. K., Lau, Y. M., Ng, K. M., Lai, W. H., Ho, S. L., Tse, H. F., Siu, C. W., and Ho, P. W. (2016) Efficient attenuation of Friedreich's ataxia (FRDA) cardiomyopathy by modulation of iron homeostasis-human induced pluripotent stem cell (hiPSC) as a drug screening platform for FRDA. *Int. J. Cardiol.* **203,** 964–971 CrossRef Medline
78. Lake, R. J., Boetefuer, E. L., Won, K. J., and Fan, H. Y. (2016) The CSB chromatin remodeler and CTCF architectural protein cooperate in response to oxidative stress. *Nucleic Acids Res.* **44,** 2125–2135 CrossRef Medline
79. Vuong, S., and Delgado-Olguin, P. (2018) Mouse genotyping. *Methods Mol. Biol.* **1752,** 1–9 CrossRef Medline
80. Valadez-Graham, V., Razin, S. V., and Recillas-Targa, F. (2004) CTCF-dependent enhancer blockers at the upstream region of the chicken α-globin gene domain. *Nucleic Acids Res.* **32,** 1354–1362 CrossRef Medline
81. Roy, A. R., and Delgado-Olguin, P. (2018) Visualizing the vascular network in the mouse embryo and yolk sac. *Methods Mol. Biol.* **1752,** 11–16 CrossRef Medline
82. Chi, L., Ahmed, A., Roy, A. R., Vuong, S., Cahill, L. S., Caporiccio, L., Sled, J. G., Caniggia, I., Wilson, M. D., and Delgado-Olguin, P. (2017) G9a controls placental vascular maturation by activating the Notch pathway. *Development* **144,** 1976–1987 CrossRef Medline
83. Delgado-Olguín, P., Dang, L. T., He, D., Thomas, S., Chi, L., Sukonnik, T., Khyzha, N., Dobenecker, M. W., Fish, J. E., and Bruneau, B. G. (2014) Ezh2-mediated repression of a transcriptional pathway upstream of Mmp9 maintains integrity of the developing vasculature. *Development* **141,** 4610–4617 CrossRef Medline
84. Chi, L., and Delgado-Olguín, P. (2018) Isolation and culture of mouse placental endothelial cells. *Methods Mol. Biol.* **1752,** 101–109 CrossRef Medline
85. Bolger, A. M., Lohse, M., and Usadel, B. (2014) Trimmomatic: A flexible trimmer for Illumina sequence data. *Bioinformatics* **30,** 2114–2120 CrossRef Medline
86. Dobin, A., Davis, C. A., Schlesinger, F., Drenkow, J., Zaleski, C., Jha, S., Batut, P., Chaisson, M., and Gingeras, T. R. (2013) STAR: Ultrafast universal RNA-seq aligner. *Bioinformatics* **29,** 15–21 CrossRef Medline
87. Anders, S., Pyl, P. T., and Huber, W. (2015) HTSeq—a Python framework to work with high-throughput sequencing data. *Bioinformatics* **31,** 166–169 CrossRef Medline
88. Love, M. I., Huber, W., and Anders, S. (2014) Moderated estimation of fold change and dispersion for RNA-seq data with DESeq2. *Genome Biol.* **15,** 550 CrossRef Medline
89. Huang, D. W., Sherman, B. T., and Lempicki, R. A. (2009) Systematic and integrative analysis of large gene lists using DAVID bioinformatics resources. *Nat. Protoc.* **4,** 44–57 CrossRef Medline